Experimental and numerical investigation of bubble dynamics rising through a rectangular confinement

Reza Azadi[1], Hirad Soltani[1], Reza Sabbagh[2] and David S. Nobes[1]*

[1]Applied Thermofluids Lab., University of Alberta, Department of Mechanical Engineering, Edmonton, Canada

[2]RGL Reservoir Management Inc., Calgary, Canada

*dnobes@ualberta.ca

Abstract

The motion of single bubbles in a net co-flow rising through a vertical rectangular confinement is experimentally and numerically investigated in this paper. A flow channel, varying from 22 mm × 5.84 mm to 3 mm × 5.84 mm (width × thickness) cross-sectional geometry was used in the present experimental investigation. The bubble sizes ranged from with 0.91 mm to 2.85 mm and the bubble motion was captured using a particle shadow velocimetry (PSV) measurement technique. A water/glycerol solution was used to control the continuous phase viscosity, while providing a fluid co-flow along with the flow of bubbles. Images were collected using a high-resolution, high-speed camera in a back illuminated configuration. The collected images from the experiments were processed using two image processing approaches of particle recognition to derive the bubble characteristics (size and rising velocity etc.) and particle image velocimetry (PIV) to determine the velocity vector map around the rising bubble, respectively. In addition, a coupled volume-of-fluid and level set method (VOSET) was used to numerically capture the interface of bubbles and compute the terminal velocity of them. It is shown that there is a good agreement between numerical and experimental results. Based on the results, for bubbles with diameters more than 1.56 mm, increasing the bubble diameter decreases its terminal velocity.

1 Introduction

Investigation of gas-liquid flows are important due to their applications in many industries, such as bubble columns, heat exchangers, environmental studies, petroleum or water pipe lines (Clift, Grace, & Weber, 1978). Dispersion of bubbles and oil droplets in a liquid medium leads to mass and heat transfer, which is the basis of fluid-fluid extraction (Komrakova, Eskin, & Derksen, 2013). Shape regime and terminal velocity of rising bubbles depends on properties of both phases such as density, viscosity, surface tension, fluid impurity, and the dispersed phase's shape and size (Kulkarni & Joshi, 2005). Typically, flow of two-phase gas-liquid fluids, in a confinement, such as circular tubes or rectangular channels are described based on the interactions between drag, gravity and surface tension forces. Single bubbles rising through unconfined channels have been widely studied (Bhaga & Weber, 1981; Böhm, Kurita, Kimura, & Kraume, 2014); some authors have predicted terminal velocity of air bubbles passing through rectangular channels (Böhm et al., 2014). However, little quantitative information on the bubble rising velocity as passing thorough a straight mini-slot inside a rectangular flow channel appears in the literature.

To investigate the effect of diameter on a bubbles terminal velocity, motion of seven different bubbles with diameters ranging from 0.91 mm to 2.85 mm were studied. Particle shadow velocimetry (PSV) was used to monitor bubble size and velocity experimentally, particle image velocimetry (PIV) was used to extract the velocity field around bubbles experimentally. VOSET method was used to simulate the fluid flow and bubble characteristics numerically. For each size, the bubble terminal velocity was computed and compared to experimental results.

2 Experimental Setup

An experimental setup was developed to investigate the velocity field in the flow surrounding bubbles rising through a vertical rectangular confining geometry. To hinder the bubble rising velocity in the bulk fluid and hence being able to capture the bubble motion in the experiments, a water/glycerol solution of 93 wt% concentration was used as the working fluid to provide a relatively high dynamic viscosity of 0.4 Pa.s. The configuration allowed the passage of the bubble through a vertical confinement designed inside a flow channel.

The bulk rate of the co-flow is addressed as a fluid flux defined as:

$$q = \frac{Q}{A} \tag{1}$$

where q is the fluid flux, Q is the volumetric flow rate and A is the cross-sectional area. Here, one fluid flux of 2.64 mm/s for the bulk flow was provided to flow along with the bubbles.

A back-light illumination approach or PSV was employed to capture the motion of bubbles rising through the rectangular confinement. Figure 1(a) shows a schematic of a shadowgraph setup for the experiments. The optical setup contained a high speed camera (CMOS SP - 5000M – PMCL, JAI Inc.) with 2560 pixel × 2048 pixel resolution and capable of capturing up to 134 frames-per-second along with a macro lens (Sigma 105 mm f/2.8 EX DG) and an LED (BX0404, Advanced Illumination Inc.) source to provide illumination. The camera was operated with an exposure time of 30 µs to freeze the bubble motion and camera frame rate was controlled using a function generator (AFG3021B, Tektronics Inc.). The LED source was aligned with the camera on the same optical axis at the back of the flow cell to provide uniform illumination over the region of interest. The experimental configuration provided a field-of-view of 8 mm × 9 mm to investigate the flow around the rising bubbles.

(a)   (b)
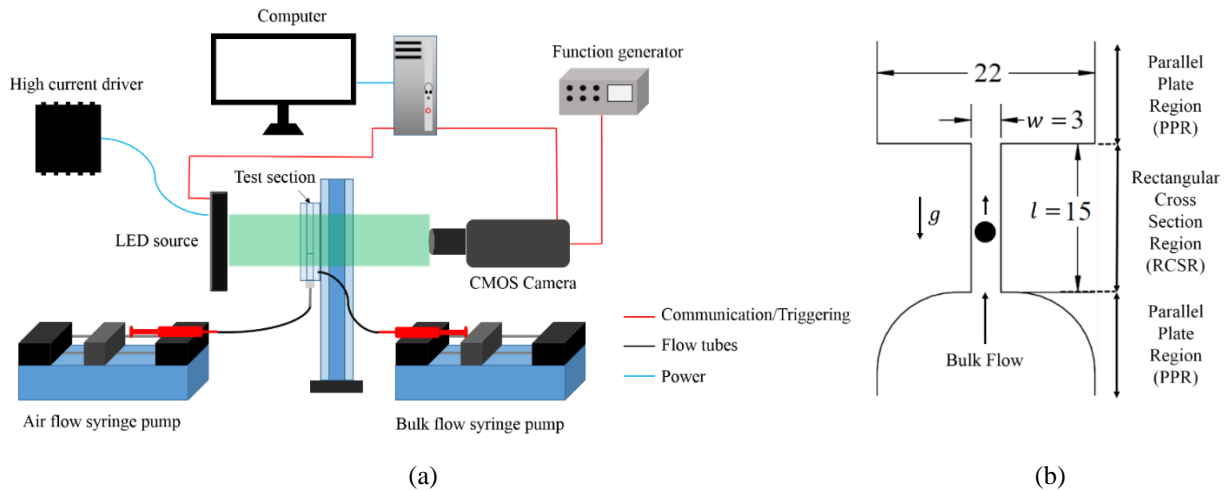
Figure 1: The (a) schematic of the shadowgraph experimental setup, and (b) details of the two-dimensional flow geometry, which has a constant depth of 5.84 mm. All dimensions are in mm.

Figure 1(b) shows the different flow regions in the flow cell including a parallel plate region (PPR) (22 mm × 5.84 mm, width × thickness) before and after a rectangular cross sectional region (RCSR) (3 mm × 5.84 mm, width × thickness) which was the focus of this study. The flow cell was mounted vertically in the experimental setup and the bulk flow direction was opposite to gravity. The flow channel (5.84 mm depth, Optix acrylic; Plaskolit Inc.) was manufactured using a commercial laser cutter (VersaLaser VLD Version 3.50; Universal Laser Systems) which provided flexibility in shaping the geometry of the flow channel and hence the experimental design. An inlet orifice of 4 mm diameter was used to inject the working fluid into the flow channel via the rear window relative to the camera view and a similar orifice was used

for the flow outlet. An inlet tube was connected to a syringe which was mounted on a syringe pump ('11' Plus, Harvard Apparatus Inc.). Air was injected through a nozzle into the fluid medium to create a bubble.

Hollow glass sphere particles (7 μm diameter) of 1.10 ± 0.05 g/cc density were mixed in the glycerol/water solution before injecting into the flow cell as tracer particles to study the motion of the fluid around the rising bubble. After mixing the tracer particles into the working fluid, the solution was left stationary for 48 hours to separate particles of relatively heavier and lighter weight than the fluid. The mixture of the fluid and tracer particles at the middle of the solution was used in experiments. This resulted in tracer particles of 1 to 3 pixels in size in the images captured in the experiment.

3 Image Processing

Shadowgraph processing was employed to quantify the diameter and rising velocity of air bubbles in different locations of the flow channel. In this step, the software (Davis 8.4.0, LaVision GmbH) recognizes bubbles based on image intensity difference between the fluid medium and bubbles. After detecting the bubble area, which has relatively less image intensity, the software calculates the number of pixels in the projected image. This was converted into physical dimensions and finds an equivalent area diameter based on the assumption that the bubble is a sphere. A minimal filter was also used to determine the desired diameter range of particles that software should recognize. This eliminates bubbles of smaller sizes and gives out information only on bubbles in the desired diameter range.

In PIV processing (Davis 8.4.0, LaVision GmbH), to brighten the tracer particles and eliminate non-uniform light intensity, image intensity was inverted and a "subtract sliding background" option was utilized, respectively. Multi-pass cross correlation with decreasing interrogation window size processing scheme was used to determine the velocity field in the bulk flow. A large interrogation window of 128 pixel × 128 pixel was chosen to capture large changes in the velocity field followed by a 64 pixel × 64 pixel window. First and second interrogating windows were used with three and one passes respectively, and 75 % window overlap in between sequential correlations.

4 Numerical Model

To numerically track the interface between two phases, a Lagrangian or Eulerian approach can be used. In the Lagrangian method, the interface is discretized and advected by interpolation of background velocity onto the interface (Hua, Stene, & Lin, 2008). In contrast, in Eulerian approach the interface is advected on one fixed mesh and is not discretized separately. Among all of the versions of the Eulerian approach, Volume of Fluid (VOF) (Rudman, 1997) and Level Set (LS) (Sussman, Smereka, & Osher, 1994) are two well-known methods. The VOF method is mass conserved but does not capture sharp interfaces, while LS method captures sharp interfaces, but is not mass conserved. To take advantage of both algorithms, both methods can be coupled (Sussman & Puckett, 2000). Sun & Tao (2010) developed the VOSET method, which couples VOF and LS methods. A modified version of VOSET was used by Ansari, Azadi, & Salimi (2016) to predict the topology of bubble motions in a stagnant fluid. VOSET uses a geometrical algorithm, which reduces the complexity of coupled coding and has proven to give results as precise as other coupled methods such as CLSVOF (Ansari et al., 2016).

Both phases are assumed as Newtonian and incompressible with no slip velocity on the interface. With this assumption, one set of Navier-Stokes equations can be written for the homogenous mixture as:

$$\boldsymbol{\nabla} \cdot \mathbf{V} = 0 \tag{2}$$

$$\rho_m \left(\frac{\partial \mathbf{V}}{\partial t} + \boldsymbol{\nabla} \cdot \mathbf{V}\mathbf{V} \right) = -\boldsymbol{\nabla} p + \boldsymbol{\nabla} \cdot [\mu_m (\boldsymbol{\nabla} \mathbf{V} + (\boldsymbol{\nabla} \mathbf{V})^T)] + \mathbf{F}_s + \mathbf{F}_g \tag{3}$$

where, $\mathbf{V} = u\mathbf{i} + v\mathbf{j}$ is the velocity and p is the pressure of the mixture. ρ and μ are density and viscosity of the mixture, respectively. $\mathbf{F}_s$ and $\mathbf{F}_g$ are surface tension and gravitational forces acting on the flow.

Density and viscosity are defined as:

$$\rho_m = \tilde{\phi}\rho_c + (1 - \tilde{\phi})\rho_d \tag{4}$$

$$\mu_m = \tilde{\phi}\mu_c + (1 - \tilde{\phi})\mu_d \tag{5}$$

where the subscripts c and d represent the continuous and dispersed phases, respectively. The Heaviside function, $\tilde{\phi}$, can be defined as (Sussman et al., 1994):

$$\tilde{\phi} = H_\epsilon(\phi) = \begin{cases} 0 & \phi < -\epsilon \\ 0.5\left[1 + \dfrac{\phi}{\epsilon} - \dfrac{1}{\pi}\sin\left(\dfrac{\pi\phi}{\epsilon}\right)\right] & |\phi| \leq \epsilon \\ 1 & \phi > \epsilon \end{cases} \tag{6}$$

where ϕ is the distance function and is obtained geometrically for each cell based on values of volume of fluid, α. The details of this coupling can are reported in the literature (Ansari et al., 2016; Sun & Tao, 2010).

The surface tension force is computed using continuum surface force (CSF) (Brackbill, Kothe, & Zemach, 1992) as:

$$\mathbf{F}_s = \sigma\kappa(\phi)\delta_\epsilon(\phi)\mathbf{n} \tag{7}$$

where σ is the surface tension coefficient, κ is the curvature of the interface and is defined as $\kappa = \nabla \cdot \mathbf{n}$. $\delta_\epsilon = dH_\epsilon/d\phi$ is the smoothed delta function and normal vector is $\mathbf{n} = \nabla\phi/|\nabla\phi|$.

For the VOSET method, first the advection equation:

$$\frac{\partial \alpha}{\partial t} + \nabla \cdot (\mathbf{V}\alpha) = 0 \tag{8}$$

is solved using the well-known Young-PLIC algorithm (Sun & Tao, 2010), then the distance function of LS method is calculated using a geometrical procedure. Knowing the distance function, the surface tension force and physical properties of the mixture flow are computed and finally are introduced to Navier-Stokes equations to solve for pressure and velocity of the flow. The location of the interface is where $\alpha \approx 0.5$ or $\phi \approx 0$.

5 Results and discussion

Figure 2 plots the bubble terminal velocity from the experimental and numerical results versus the bubble sizes. In this plot, V_{t-RCSR} is the bubble terminal velocity through the RCSR and D_e is the bubble equivalent diameter, which is normalized to the RCSR width, w. A mesh size of $0.034w$ in both x and y directions was used to simulate the bubble motion. A velocity-inlet boundary condition was applied to the channel inlet, the outlet of the channel had a pressure-outlet boundary condition and no-slip wall boundary condition was applied to the channel walls. The maximum and minimum deviation between the experimental and numerical data were calculated as 11.85% for bubble diameter 2.36 mm and 1.68% for diameter 1.56 mm, respectively. Figure 2 indicates that for bubble sizes larger than 1.5 mm, the bubble terminal velocity decreases as the diameter is increased due to confining wall effects.

The bubble terminal velocity can be derived from the vertical velocity component in the whole domain to develop a pseudo-Lagrangian velocity vector field for both experimental and numerical results. These velocity vectors are plotted in Figure 3(a) and 3(b), respectively. In Figure 3(a), y and x are the lengthwise and horizontal distances in the RCSR, which are normalized to the RCSR width, w. Qualitative comparison of the experimental and numerical results of the velocity field around rising bubbles shows that in front of and behind the bubble, both approaches give approximately the same result. The actual three-dimensional flow was modelled in two-dimensions, meaning that the confinement effects in the third direction are

neglected. This can be a reason that the numerical simulations predict a relatively stronger circulation between the bubble and confining walls. This is more evident for the fluid between the bubble and the confinement walls, where the changes in the velocity magnitude does not follow the experimental results.
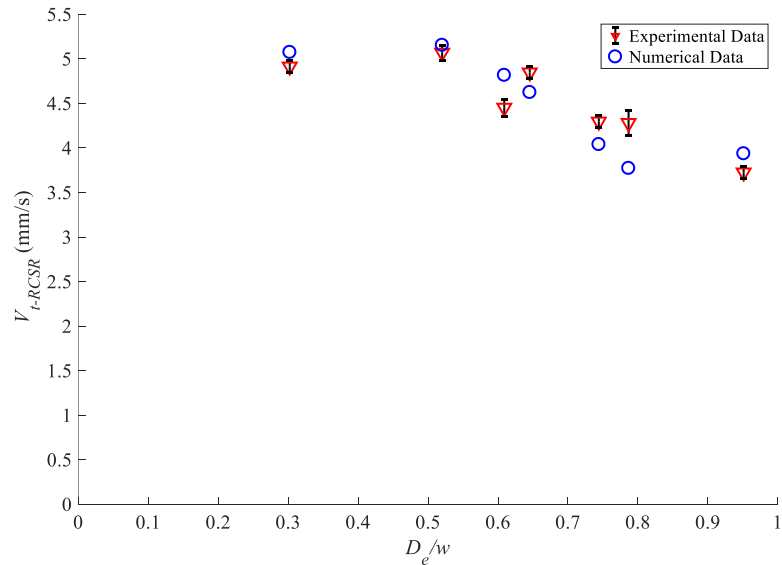
Figure 2 Experimental and numerical results for the bubble terminal velocity for q = 2.64 mm/s.

(a)   **(b)**
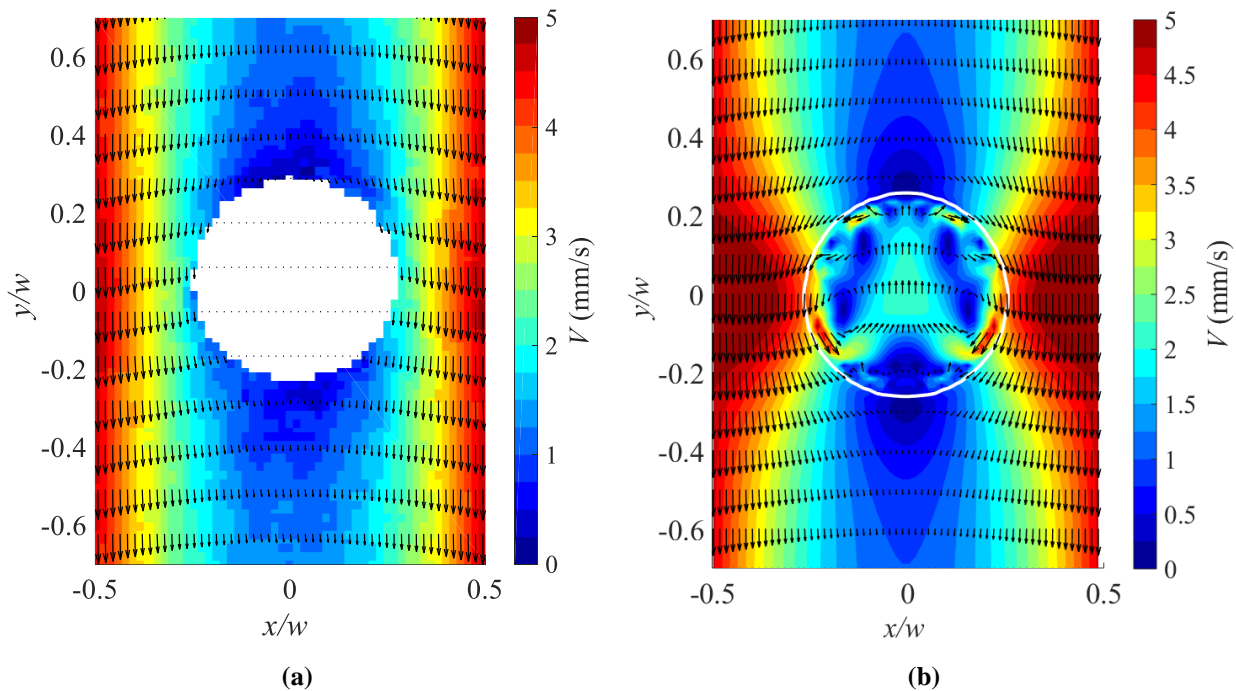
Figure 3 Pseudo-Lagrangian velocity vectors around a bubble with D_e =1.56 mm from the (a) Experimental PIV, and (b) Numerical VOSET results, where the white edge shows the interface between the phases. q =2.64 m/s. The vector fields for both plots show only every 3rd and 6th vectors in the horizontal and vertical directions, respectively.

6 Conclusion

Motion of bubbles in a viscous flow inside a confined channel were investigated experimentally and numerically. Using PIV, the velocity field around the rising bubbles were extracted from high-resolution images. To simulate the flow numerically, coupled VOSET method was used. Both experimental and numerical results showed that for bubbles with diameters above 1.5 mm, terminal velocity decreases with increasing the bubble diameter due to the confining wall effect. In general, the characteristic of the flow were captured by the numerical model, however, variations in the results in the near wall region require additional investigation.

Acknowledgements

References

Ansari MR, Azadi R, and Salimi E (2016) Capturing of interface topological changes in two-phase gas-liquid flows using a coupled volume-of-fluid and level-set method (VOSET). *Computers and Fluids* 125:82–100.

Bhaga D, and Weber ME (1981) Bubbles in viscous liquids: Shapes, wakes and velocities. *Journal of Fluid Mechanics* 105:61–85.

Böhm L, Kurita T, Kimura K, and Kraume M (2014) Rising behaviour of single bubbles in narrow rectangular channels in Newtonian and non-Newtonian liquids. *International Journal of Multiphase Flow* 65:11–23.

Brackbill J., Kothe D., and Zemach C (1992) A continuum method for modeling surface tension. *Journal of Computational Physics* 100:335–354.

Clift R, Grace JR, and Weber ME (1978) *Bubbles, Drops and Particles* (Vol. 94). New York; London: Academic Press.

Hua J, Stene JF, and Lin P (2008) Numerical simulation of 3D bubbles rising in viscous liquids using a front tracking method. *Journal of Computational Physics* 227:3358–3382.

Komrakova AE, Eskin D, and Derksen JJ (2013) Lattice Boltzmann simulations of a single n-butanol drop rising in water. *Physics of Fluids* 25:42102.

Kulkarni A a, and Joshi JB (2005) Bubble Formation and Bubble Rise Velocity in Gas - Liquid Systems : A Review. *Industrial & Engineering Chemistry Research* 44:5873–5931.

Rudman M (1997) VOLUME-TRACKING METHODS FOR INTERFACIAL FLOW CALCULATIONS. *International Journal for Numerical Methods in Fluids* 24:671–691.

Sun DL, and Tao WQ (2010) A coupled volume-of-fluid and level set (VOSET) method for computing incompressible two-phase flows. *International Journal of Heat and Mass Transfer* 53:645–655.

Sussman M, and Puckett EG (2000) A Coupled Level Set and Volume-of-Fluid Method for Computing 3D and Axisymmetric Incompressible Two-Phase Flows. *Journal of Computational Physics* 162:301–337.

Sussman M, Smereka P, and Osher S (1994) A Level Set Approach for Computing Solutions to Incompressible Two-Phase Flow. *Journal of Computational Physics* 114:146–159.